

A Journal of the Gesellschaft Deutscher Chemiker

Angewandte Chemie

GDCh

International Edition

www.angewandte.org

Accepted Article

Title: Long-cycling and High-voltage Solid State Lithium Metal Batteries Enabled by Fluorinated and Crosslinked Polyether Electrolytes

Authors: Jie Zhu, Ruiqi Zhao, Jinping Zhang, Xingchen Song, Jie Liu, Nuo Xu, Hongtao Zhang, Xiangjian Wan, Xinyi Ji, Yanfeng Ma, Chenxi Li, and Yongsheng Chen

This manuscript has been accepted after peer review and appears as an Accepted Article online prior to editing, proofing, and formal publication of the final Version of Record (VoR). The VoR will be published online in Early View as soon as possible and may be different to this Accepted Article as a result of editing. Readers should obtain the VoR from the journal website shown below when it is published to ensure accuracy of information. The authors are responsible for the content of this Accepted Article.

To be cited as: *Angew. Chem. Int. Ed.* **2024**, e202400303

Link to VoR: <https://doi.org/10.1002/anie.202400303>

Long-cycling and High-voltage Solid State Lithium Metal Batteries Enabled by Fluorinated and Crosslinked Polyether Electrolytes

Jie Zhu,^{[a],[c]} Ruiqi Zhao,^{[a],[c]} Jinping Zhang,^{[a],[c]} Xingchen Song,^{[a],[c]} Jie Liu,^{[a],[c]} Nuo Xu,^{[a],[c]} Hongtao Zhang,^{[a],[c],*} Xiangjian Wan,^{[a],[b],[c]} Xinyi Ji,^{[d],*} Yanfeng Ma,^{[a],[c]} Chenxi Li,^{[a],[c]} and Yongsheng Chen^{[a],[b],[c],*}

^[a] The Centre of Nanoscale Science and Technology and Key Laboratory of Functional Polymer Materials, Institute of Polymer Chemistry, College of Chemistry, Nankai University, Tianjin 300071, China

^[b] State Key Laboratory of Elemento-Organic Chemistry, Nankai University, Tianjin, 300071, China

^[c] Renewable Energy Conversion and Storage Center (RECAST), Nankai University, Tianjin 300071, China

^[d] School of Materials Science and Engineering, National Institute for Advanced Materials, Nankai University, Tianjin, 300350, China

Corresponding E-mails: yschen99@nankai.edu.cn; htzhang@nankai.edu.cn; xyji06@nankai.edu.cn

Abstract: Solid-state lithium metal batteries (LMBs), constructed through the in-situ fabrication of polymer electrolytes, are considered a critical strategy for the next-generation battery systems with high energy density and enhanced safety. However, the constrained oxidation stability of polymers, such as the extensively utilized polyethers, limits their applications in high-voltage batteries and further energy density improvements. Herein, an in-situ fabricated fluorinated and crosslinked polyether-based gel polymer electrolyte, FGPE, is presented, exhibiting a high oxidation potential (5.1 V). The fluorinated polyether significantly improves compatibility with both lithium metal and high-voltage cathode, attributed to the electron-withdrawing $-\text{CF}_3$ group and the generated LiF-rich electrolyte/electrode interphase. Consequently, the solid-state $\text{Li}||\text{LiNi}_{10.6}\text{Co}_{0.2}\text{Mn}_{0.2}\text{O}_2$ batteries employing FGPE demonstrate exceptional cycling performances of 1000 cycles with 78% retention, representing one of the best results ever reported for polymer electrolytes. Moreover, FGPE enables batteries to operate at 4.7 V, realizing the highest operating voltage of polyether-based batteries to date. Notably, our designed in-situ FGPE provides the solid-state batteries with exceptional cycling stability even at practical conditions, including high cathode loading (21 mg cm^{-2}) and industry-level 18650-type cylindrical cells (1.3 Ah, 500 cycles). This work provides critical insights into the development of oxidation-stable polymer electrolytes and the advancement of practical high-voltage LMBs.

Introduction

After decades of commercialization, graphite anodes are approaching their theoretical capacity limit of 372 mAh g⁻¹, yet fall short in meeting the ever-growing demands of energy density for electronic equipment.^[1] Therefore, the lithium metal anode (LMA) has emerged as a potential candidate in next-generation battery systems, attributed to its high theoretical specific capacity (3860 mAh g⁻¹) and low redox potential (-3.04 V vs. the standard hydrogen electrode).^[2] However, the highly reactive LMA leads to uncontrollable lithium dendrite growth and electrolyte consumption, resulting in limited lifespan and severe safety hazards.^[3] Polymer electrolytes, characterized by non-leakage, easy processing, and flexibility, are considered promising solid-state electrolytes to address these issues and enable high-energy-density batteries.^[4] Among various polymer electrolytes, polyether-based electrolytes exhibit excellent reduction stability and efficient ion transport ability benefited from the exceptional coordination and disassociation ability of the C–O–C groups with lithium salts. Therefore, they are extensively utilized and well-suited for lithium metal batteries (LMBs).^[5]

Moreover, using prevailing Ni-rich layered oxide cathodes, LiNi_{1-x-y}Co_xMn_yO₂ (NCM: 1-x-y ≥ 0.6), is an effective strategy to further exploit the energy density of LMBs, owing to their high theoretical capacity, high operating voltage, and low cost. However, polyether-based electrolytes are not compatible with Ni-rich NCM cathodes due to their oxidative decomposition resulted from the unstable lone-pair electrons in the ether oxygen bonds.^[6] Furthermore, the aggressive high-valence nickel in the NCM cathode will further aggravate the decomposition of electrolyte, resulting in an uneven cathode electrolyte interphase (CEI) with large interfacial resistance and poor conductivity.^[7] It can be concluded that the poor oxidation stability and undesirable CEI of polyether-based electrolytes constitute their fundamental weakness in pairing with high-voltage cathodes, particularly Ni-rich NCM cathodes, which limits further improvements in energy density of LMBs.

To date, several strategies have been proposed to tackle the high-voltage stability problem of polyether-based electrolytes, including: 1) the replacement of the unstable terminal –OH group of polyether with a more stable group (–OCH₃);^[8] 2) the elimination of the –OH group with inferior oxidation stability by crosslinking;^[9] 3) the use of electrolyte additives to modify the CEI;^[10] and 4) the incorporation of inorganic fillers which involves the interaction between the surface of the filler and the lone-pair electrons of the polyether.^[5a, 11] These strategies have been demonstrated to achieve satisfactory cycling performance when pairing with Ni-rich NCM cathodes. However, the unstable ether oxygen bond, a critical factor limiting the oxidation stability of polyether, remains unaddressed.^[6a] Therefore, it is still

challenging for polyether-based batteries to operate under a high cut-off potential, particularly above 4.3 V. Introducing fluorine atoms or fluorinated functional groups has proven to be a more effective strategy to enhance the oxidation resistance of polymer electrolytes.^[3b, 12] For instance, Zhou et al. reported a fluorinated poly-oxalate electrolyte, providing all-solid-state Li||LiNi_{0.8}Co_{0.1}Mn_{0.1}O₂ (NCM811) batteries with significantly improved stability.^[12b] Du et al. reported a fluorinated poly-acrylate electrolyte, and the fabricated Li||LiNi_{0.6}Co_{0.2}Mn_{0.2}O₂ (NCM622) batteries using this electrolyte exhibited excellent cycling stability even at 4.5 V.^[3b] In addition to oxidation stability, fluorination also enhances lithium metal compatibility by generating LiF-containing solid electrolyte interphase (SEI).^[13] However, there have been no studies reporting on fluorinated polyether electrolytes and the prepared batteries operating with a high cut-off voltage (≥ 4.5 V). Therefore, the development of an oxidation-stable polyether electrolyte by fluorination is anticipated, which can simultaneously contribute to high-quality high-quality CEI/SEI and ultimately enable high-voltage LMBs with superior cycling stability.

In this work, we propose a novel strategy for fabricating a fluorinated and crosslinked polyether-based electrolyte (FGPE) through in-situ cationic ring-opening polymerization of fluorinated monomer and four-armed cross-linker within the battery. The in-situ crosslinking method ensures intimate interfacial contact.^[14] The obtained three-dimensional crosslinked polymer network facilitates high solvent uptake, achieving a high ionic conductivity of up to 3.98 mS cm⁻¹. Most importantly, after fluorination, the oxidation stability of polyether is significantly improved, exhibiting a high oxidation potential of up to 5.1 V. The incorporation of fluorinated group promotes the formation of fluorinated SEI and CEI, subsequently enhancing lithium metal stability and high-voltage tolerance. As a result, the assembled Li||NCM622 battery based on our developed FGPE demonstrates an ultra-long cycling performance of 1000 cycles with 78% capacity retention at 4.3 V, which is the best result among all the reported polymer electrolyte-based batteries. When operating at 4.7 V, the FGPE-based battery achieves a high specific capacity of over 210 mAh g⁻¹, realizing the first instance of polyether-based battery operating at such a high voltage. Importantly, the fluorinated and crosslinked polyether electrolyte can be applied in a solid-state lithium metal pouch cell with high cathode mass loading of 21 mg cm⁻², demonstrating stable cycling performance of 100 times. The practical application of FGPE is further highlighted by fabricating an industry-level 1.3-Ah 18650 cylindrical cell and achieving an excellent cycling stability of 500 times. This work provides new insights for designing oxidation-stable polymer electrolytes, and developing practical high-voltage LMBs.

Temperature dependence of the ionic conductivity of FGPE and GPE. The data were fitted by the Arrhenius transport model.

To evaluate the electrochemical redox activities of the fluorinated and non-fluorinated polymer network, density functional theory (DFT) calculations were conducted (Figure 1b). Compared to non-fluorinated p(DOL-PEE), the fluorinated p(TFPO-PEE) exhibits a relatively lower highest occupied molecular orbital (HOMO) due to the electron-withdrawing trifluoromethyl group, demonstrating an improved anti-oxidation ability. Moreover, the p(TFPO-PEE) also exhibits a relatively low lowest unoccupied molecular orbital (LUMO), indicating its preferential reduction at the anode and participation in the formation of the robust SEI. The electrochemical stability of electrolytes was analyzed by linear sweep voltammetry (LSV) measurement. As shown in Figure 1c, FGPE displays a high oxidation potential of up to 5.1 V, which significantly exceeds that of non-fluorinated GPE, attributed to the incorporation of fluorinated functional groups. Temperature dependence of the ionic conductivity of FGPE and GPE is presented in Figure 1d. At room temperature (25 °C), the ionic conductivity of FGPE reaches a high value of 3.98 mS cm⁻¹, surpassing that of GPE (2.63 mS cm⁻¹, Figure S2). When fitting the data by the Arrhenius equation, FGPE displays a lower activation energy barrier of 12.76 kJ mol⁻¹ compared to GPE, which can facilitate the transport of Li⁺. FGPE also shows a high transference number (t_{Li^+}) of 0.59 (Figure S3), which can effectively reduce the concentration polarization of Li⁺, and thus inhibit Li dendrites growth, resulting in improved battery performance.

The stability between electrolyte and lithium metal is critical to achieving the long-cycling performance of batteries. As shown in Figure 2a, Li||Li symmetric cells were assembled to test the interfacial stability during Li planting/stripping. Under a current density of 0.5 mA cm⁻² with the area capacity of 0.5 mAh cm⁻², the Li|FGPE|Li symmetric cell exhibits an exceptionally stable cycling with a small overpotential (35 mV) for 2000 h. In contrast, the short circuit of Li||Li symmetric cells using GPE and LE occurs after 378 and 614 h, respectively. The improved cycling performance of Li|FGPE|Li symmetric cell indicates an enhanced stability of lithium planting/stripping in the FGPE. To verify this, the lithium metal stability was further assessed via the Coulombic efficiency (CE) and deposition morphology in Li||Cu cells.^[15] As shown in Figure S4, the Li|FGPE|Cu cell delivers a steady cycling with a high CE of 97.5%, while the Li||Cu cells using GPE and LE present lower CEs (95.2% and 94.37%) with obvious oscillation, implying the satisfactory compatibility of FGPE towards LMAs. The morphologies of deposited lithium in Li||Cu cells were investigated by scanning electron microscopy

(SEM). As shown in Figure 2b, the lithium deposited in FGPE displays a compact and large granular morphology, effectively alleviating the parasitic reactions between FGPE and lithium. In contrast, the deposited lithium in GPE and LE shows a loose and long tubular lithium structure (Figure 2c and S5). All these together demonstrate the high reversibility of lithium planting/stripping in FGPE. Furthermore, critical current density (CCD) was applied to evaluate the Li dendrite-suppression capability of FGPE (Figure 2b). Due to the higher ionic conductivity and improved interfacial stability, the FGPE exhibits a high CCD of 4 mA cm^{-2} , while the GPE without fluorinated structure limits its CCD to 3 mA cm^{-2} (Figure S6). Moreover, Li|FGPE|Li symmetric cell exhibits superior rate performance, with overpotentials of 22.4, 37.4, 63.6, 99.4, and 140.5 mV at current densities of 0.5, 1, 2, 3, and 4 mA cm^{-2} , respectively (Figure S7). This performance significantly surpasses that of the non-fluorinated GPE, which has a lower CCD of 3 mA cm^{-2} , as demonstrated in Figure S6.

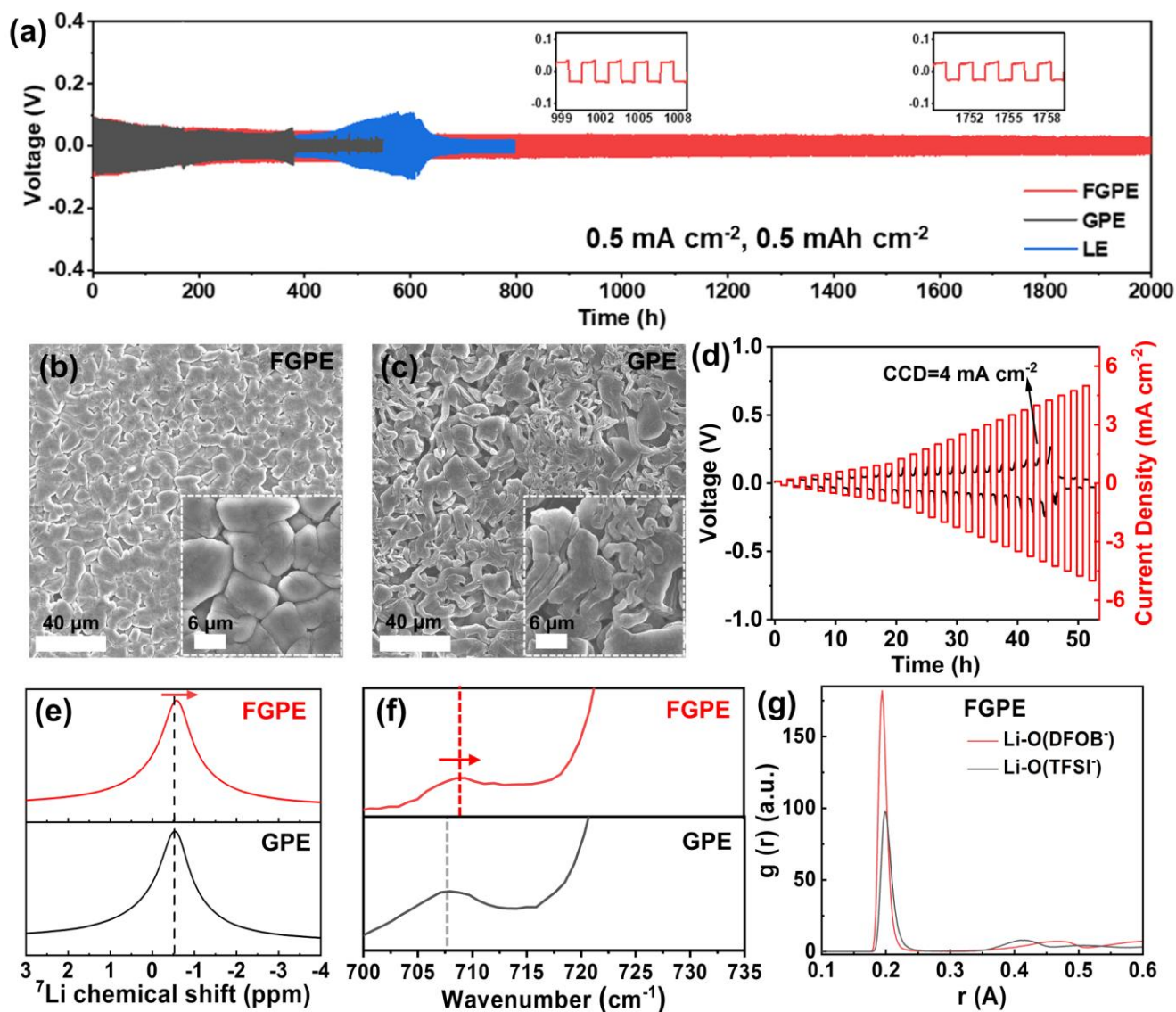


Figure 2. (a) Polarization tests of Li||Li symmetric cells with FGPE, GPE, and LE at 0.5 mA cm^{-2} and 0.5 mAh cm^{-2} . SEM images of Li deposition after planting 5 mAh cm^{-2} on the Cu current collector in Li||Cu asymmetric cells using (b) FGPE and (c) GPE. (d) Critical current density test of the symmetric Li|FGPE|Li cell. (e) Comparison of ^7Li ssNMR spectra of FGPE and GPE. (f) Raman spectra of FGPE and GPE from 700 cm^{-1} to 735 cm^{-1} . (g) Radial distribution function in molecular dynamics simulation of the FGPE.

Considering the reversibility of lithium plating/stripping and the properties of SEI are highly associated with the solvation structure, ^7Li ssNMR and Raman spectra were conducted to unveil the solvation structure of FGPE. The chemical shift in ^7Li ssNMR reflects the shielding of Li^+ that results from the solvation structure.^[16] As shown in Figure 2e, FGPE displays a more negative chemical shift (-0.580 ppm) than GPE (-0.519 ppm). The upfield shift of FGPE demonstrates the increase in electron density around Li^+ , which results in a relatively strong shielding of Li^+ , indicating the stronger interaction between the anions and Li^+ . The Raman spectrum provides further solvation structure information of FGPE. The peaks found in the range of $700\text{-}720 \text{ cm}^{-1}$ and $730\text{-}750 \text{ cm}^{-1}$ in Figure 2f and Figure S8 correspond to the ring-breathing vibration of the difluoro(oxalate)borate anion (DFOB^-)^[17] and the S–N–S stretching vibration of the bis(trifluoromethanesulfonyl)imide anion (TFSI^-)^[18] respectively. Compared to GPE, FGPE exhibits a blue shift due to the increased coordination between anions and Li^+ ,^[19] which is in consistent with the results of ^7Li ssNMR. Besides the spectral analysis method, theoretical calculation based on molecular dynamics (MD) simulation was conducted to prove the stronger interaction between the anions and Li^+ in FGPE. Figure 2g and Figure S9 exhibit the radial distribution function (RDFs) of Li^+ to DFOB^- and TFSI^- in different electrolytes. The Li–O(DFOB^-) and Li–O(TFSI^-) present higher frequencies (the absolute value of $g(r)$) in FGPE than in GPE, demonstrating that the anions are more probable to enter the first solvation sheath of Li^+ in FGPE.^[20] The anion-rich solvation structure in FGPE can promote the formation of an inorganic-rich and stable SEI on the anode, which contributes to the enhanced lithium metal stability. As shown in Figure S10, X-ray photoelectron spectroscopy (XPS) depth profiling using Ar ion etching was performed to investigate the three-dimensional composition of the interfacial components of the Li anode. In the F 1s spectra, comparing with the non-fluorinated GPE, the surface composition of the lithium deposited in FGPE contains more LiF, due to the anion-rich solvent structure and the fluorinated polymer network.^[21] Moreover, in the N 1s spectra, the higher content of nitrogen-containing species (Li_3N and LiN_xO_y) in FGPE system represents a more sufficient

decomposition of TFSI⁻, corroborating the positive effect of the anion-rich solvent structure.^[22] These results indicate that the gradually formed inorganic SEI components in the FGPE system, facilitated by the anion-rich solvent structure and the fluorinated polymer network, contributes to improved lithium metal stability. To further evaluate the lithium metal anode stability of FGPE, Li|FGPE|LFP battery was assembled and the cycling performance was shown in Figure S11. Due to its robust SEI and excellent compatibility with lithium metal, FGPE enables the Li||LFP battery to achieve an exceptional super-long cycling of 2000 cycles at 2 C with a high capacity retention of 81.2%, which is superior to the batteries using GPE or LE.

The superior oxidation stability of FGPE makes it compatible with high voltage cathodes, such as nickel-rich NCM622. Therefore, coin-type batteries that assembled with NCM622 as cathode and Li metal as anode were tested at high cut-off voltages (4.3-4.7 V). The cycling performances of Li||NCM622 batteries with different electrolytes at 0.5 C with a cut-off voltage of 4.3 V are shown in Figure 3a. The Li|FGPE|NCM622 battery achieves an ultra-long cycling stability of 1000 cycles with a high capacity retention of 78.0% (corresponding to a capacity decay of 0.022% per cycle). To the best of our knowledge, this is one of the best cycling performances of Li||NCM622 batteries among all the polymer electrolyte-based batteries reported so far (Figure 3e and Table S1). In contrast, without the fluorinated and crosslinked polymer network, both the Li|GPE|NCM622 and Li|LE|NCM622 batteries exhibit obvious decay after only 300 cycles, retaining 71.6% and 60.8% of their initial capacity, respectively. The corresponding charge/discharge curves of Li||NCM622 batteries using different electrolytes are also provided in Figure S12. Furthermore, the Li|FGPE|NCM622 battery delivers specific capacities of 176.3, 170.1, 161.1, 152.4, 142.3, 124.6, and 104.6 mAh g⁻¹ at 0.1 C, 0.2 C, 0.5 C, 1 C, 2 C, 5 C, and 10 C, and the capacity recovers to the initial value when turning back to 0.5 C (Figure S13). Hence, it can be concluded that the battery using FGPE possesses satisfactory rate performance.

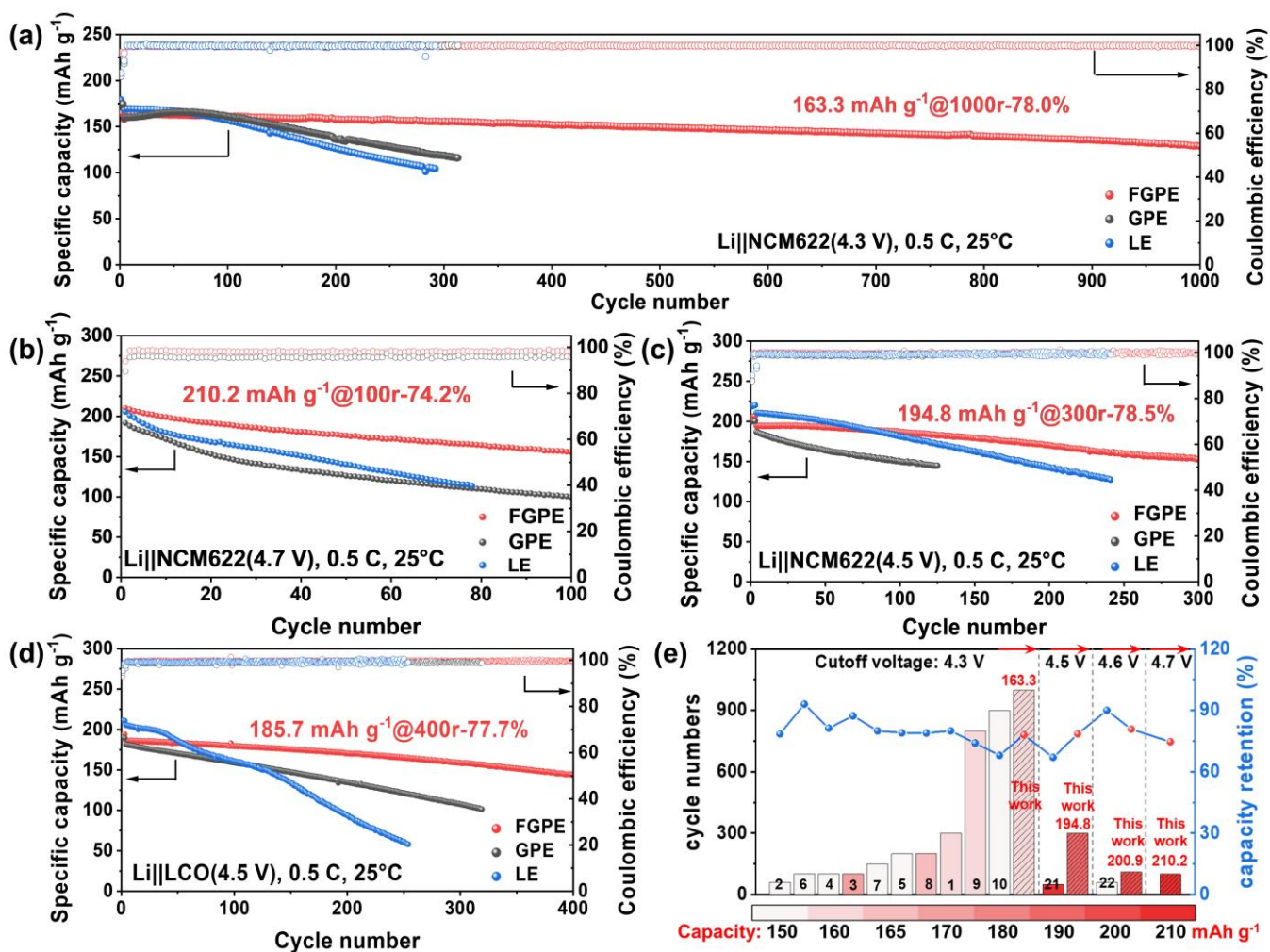


Figure 3. (a) Cycling performances of Li||NCM622 batteries using FGPE, GPE, and LE at 0.5 C at charge cut-off voltages of 4.3 V. (b) Cycling performances of Li||NCM622 batteries using FGPE and GPE at 0.5 C at charge cut-off voltages of 4.7 V. (c) Cycling performances of Li||NCM622 batteries using FGPE, GPE, and LE at 0.5 C at charge cut-off voltages of 4.5 V. (d) Cycling performances of Li||LCO batteries using FGPE, GPE, and LE at 0.5 C at a high charge cut-off voltage of 4.5 V. (e) Performance comparison of Li||NCM622 batteries using FGPE (this work) and other reported works using polyether-based electrolytes in terms of cycle numbers, capacity retention, cut-off voltage, and discharge capacity.

To further assess the high-voltage stability of FGPE, Li|FGPE|NCM622 batteries were tested at 0.5 C with various high cut-off voltages. Notably, when raising the cut-off voltage to 4.7 V, the Li||NCM622 battery based on our fluorinated and crosslinked polyether electrolyte (FGPE) achieves a high specific capacity of 210.2 mAh g⁻¹ with a high capacity retention of 74.2% after 100 cycles (Figure 3b). As far as we know, this is the first reported Li||NCM622 battery with such a high cut-off voltage of 4.7 V based on reported polyether electrolytes, confirming the excellent high-voltage stability of FGPE. At a cut-off

voltage of 4.5 V, battery using FGPE is capable of delivering a stable cycling of 300 times as shown in Figure 3c, exceeding that of battery assembled with GPE and LE. When using LCO as cathode, the Li|FGPE|LCO battery operating at 4.5 V also demonstrates an excellent long-cycling performance of 400 cycles with a high specific capacity of 185.7 mAh g⁻¹ and a high capacity retention of 77.7% (Figure 3d). In contrast, these Li||LCO batteries using GPE and LE both suffer from severe capacity decay. This rapid capacity degradation is due to the uncontrolled parasitic reactions and the resulting consumption of the electrolyte and electrode. The cycling performances of the reported polymer electrolytes-based batteries that coupled with NCM622 cathode were compared in Table S1 and S2, and Figure 3e. Our developed FGPE enables polyether-based Li||NCM622 battery to achieve a long cycling of 1000 times with a high capacity retention of 78.0% at 4.3 V, which is also the best cycling performance even among all the polymer electrolyte-based batteries. At elevated cut-off voltages of 4.5 and 4.6 V, the cycling performance of our FGPE-based battery is still superior to other reported polyether-based batteries (detailed in Figure S14). Furthermore, 4.7 V Li|FGPE|NCM622 battery is first realized based on polyether-based electrolytes. It can be concluded that this is a remarkable improvement over the prior works (Table S1 and S2, and Figure 3e), which renders a new and more effective method for developing polymer electrolytes-based high-voltage LMBs.

The critical role of FGPE in stabilizing the NCM622 cathode is further revealed. At first, electrochemical floating analysis (EFA) was performed to verify the practical interfacial compatibility of FGPE towards NCM622. By measuring the leakage current during EFA, the compatibility can be evaluated and the results are shown in Figure 4a. The Li||NCM622 battery using FGPE shows a stable leakage current in the voltage range of 4.2-4.9 V, and the leakage current is still very low (13.3 μ A) even at 4.9 V. In sharp contrast, the Li|GPE|NCM622 battery exhibits a larger and increasing current when charging at 4.5 V (Figure S15). These results demonstrate the enhanced oxidation stability of the polyether electrolyte in high-voltage batteries after fluorination. Then, SEM was employed to characterize the interface of the cycled NCM622 cathode. As shown in Figure S16, the cathode cycled with FGPE remains intact and exhibits a relatively smooth surface, while the cathodes cycled with GPE and LE show broken strips on the surface. Generally, cracking of Ni-rich cathodes is a critical issue for their degradation, particularly under high cut-off voltage and long-time cycling.^[23] The morphology of the CEI and the crystal structure of the cycled NCM622 were observed by TEM. A uniform and thin CEI layer (~5.1 nm) was observed in the FGPE system (Figure 4b), compared to a thick and non-uniform CEI in the GPE system (Figure 4c). Moreover, as shown in Figure S17, the NCM622 layer structure is well-retained with

the same lattice spacing of 4.73 Å. The uniform CEI and well-retained structure indicate the superior compatibility between high-voltage cathodes and our FGPE.

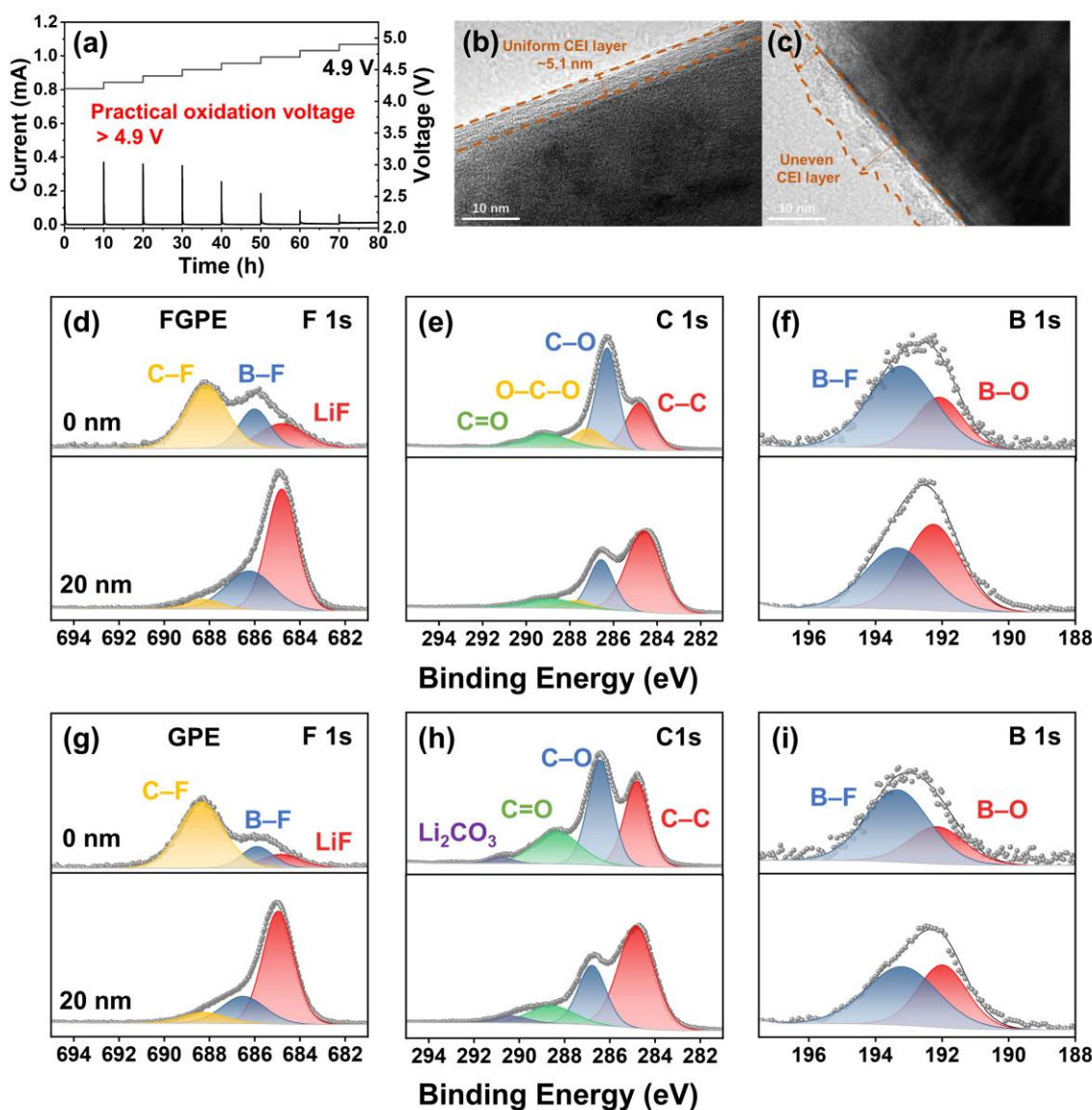


Figure 4. (a) Electrochemical floating analysis of FGPE. TEM images (b-c) and XPS depth profiles of NCM622 cathode harvested from Li||NCM622 batteries using FGPE (d-f) and GPE (g-i) after 50 cycles at 0.5 C.

As shown in Figure 4(d-i), the structure of CEI was systematically studied with XPS depth profiles. On the top surface, the CEI of NCM cathode in Li|FGPE|NCM622 battery displays a more pronounced peak of LiF (684.8 eV) in the F 1s spectra compared to the GPE system. Owing to the high oxidative resistance of LiF, the oxidative decomposition of electrolyte at high potentials could be effectively inhibited.^[24] In the B 1s spectra, a relatively stronger signal of B–O species (192.1 eV) is observed in the FGPE system, arising from the decomposition of LiDFOB on the cathode. According to previous reports,

B–O species have been proven to stabilize the surface and mitigate the corrosion of the cathode.^[25] After sputtering, the enhanced signal intensities of LiF and B–O in the FGPE system indicate an inorganic component-rich inner layer. The elevated gradient of inorganic components suppresses the decomposition of carbonate solvents, as evidenced by the reduced intensities of organic components in the C 1s spectra. In contrast, in the GPE system, the CEI exhibits higher signal intensities of C=O and Li₂CO₃ and lower signal intensity of LiF and B–O compared to FGPE system. This indicates that the CEI in GPE insufficiently inhibits carbonate solvent consumption, aligning with observations of a thick and non-uniform CEI. However, in the Li||NCM622 battery assembled with our fluorinated FGPE, a boron- and LiF-enriched protective CEI has formed. This robust CEI enhances the high-voltage stability of the Li||NCM622 battery, thus enabling the ultra-long cycling of 1000 cycles as previously mentioned.

Considering the high ionic conductivity, excellent lithium metal stability, and high voltage tolerance of FGPE, full lithium metal batteries (coin-type) were assembled and tested with high-loading NCM622 cathodes (8.7 and 21.0 mg cm⁻²) and thin lithium foil anodes (50 μm). With a high cut-off voltage of 4.5 V and a low N/P ratio of 5.7 (8.7 mg cm⁻² NCM622 cathode), the LMB using FGPE still exhibits satisfactory cycling stability (Figure 5a), delivering 190.4 mAh g⁻¹ at 0.2 C with a high capacity retention of 86.7% after 100 cycles. A high rate performance is also maintained, which delivers 191.6, 185.8, 177.3, 169.2, 155.6 and 105.9 mAh g⁻¹ at 0.1 C, 0.2 C, 0.5 C, 1 C, 2 C, and 5 C, respectively (Figure 5b).

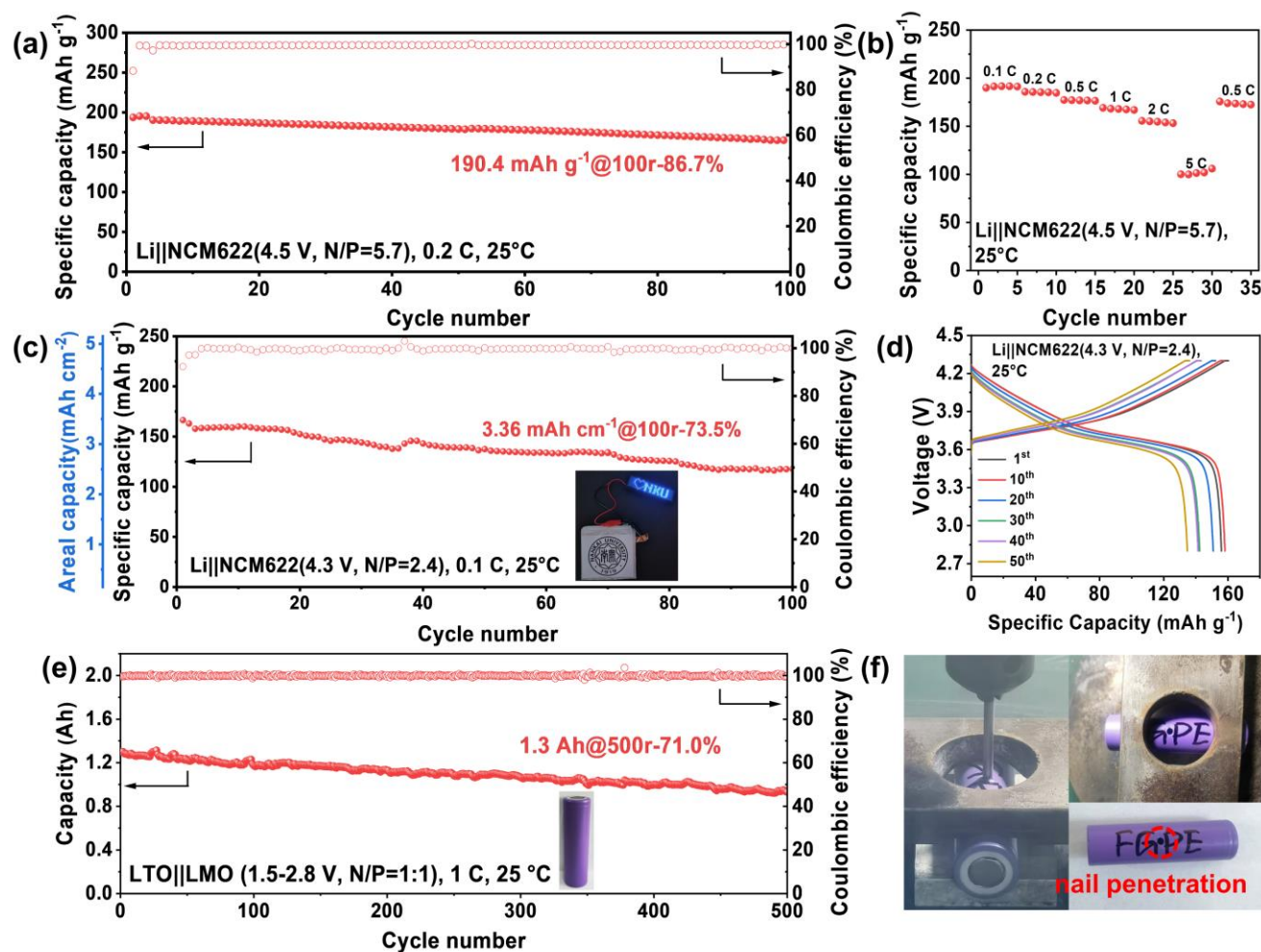


Figure 5. (a) Cycling and (b) rate performance of Li|FGPE|NCM622 batteries at a high charge cut-off voltage of 4.5 V with a low N/P ratio of 5.7. (c) Cycling performance and (d) voltage profiles of solid-state Li|NCM622 pouch cell using FGPE at a charge cut-off voltage of 4.3 V with a low N/P ratio of 2.4 (cathode mass loading: 21 mg cm^{-2}). (e) Cycling performances of a 1.3-Ah solid-state 18650 cylindrical cell using FGPE with a practical N/P ratio of 1. (f) Nail penetration test for solid-state 18650 cylindrical cell using FGPE.

To further demonstrate the potential of FGPE for practical applications, both pouch cells and coin-type cells were assembled by using high-loading NCM622 cathode (21.0 mg cm^{-2}) and thin lithium foil anode ($50 \text{ }\mu\text{m}$) with a low N/P ratio of 2.4. As shown in Figure 5c, the prepared solid-state lithium metal pouch cell exhibits a stable cycling of 100 cycles at 0.1 C (73.5% capacity retention), with a high specific capacity of 3.36 mAh cm^{-2} . The corresponding voltage profiles of the pouch cell using FGPE demonstrate low polarization and high Coulombic efficiency (Figure 5d). Pouch cell with a high capacity of 0.2 Ah was also fabricated, displaying outstanding cycling stability with a high capacity retention of 81.4% after 60 cycles at 0.1 C (Figure S14). In addition, coin-type full cell with a low N/P ratio of 2.4 using FGPE

exhibits satisfactory rate performance and cycling stability (Figure S15), delivering 160.7 mAh g⁻¹ at 0.2 C with a high capacity retention of 95.0% after 100 cycles. Moreover, the FGPE proved to possess excellent safety and reliability in the solid-state lithium metal pouch cell. Figure S16 presents the different states of the pouch cell lighting up LED lamps. Upon bending, piercing, and cutting, no burning or explosion occurred and the LED lamps remained illuminated.

Furthermore, the practicability of FGPE was investigated at the industry-level of 18650 cylindrical cells. 18650 cell is the most ubiquitous cell geometry that is widely used in electric vehicles and power banks.^[26] However, to the best of our knowledge, there are scarce reports about solid-state 18650 cylindrical cells. In this work, we fabricated a solid-state 18650 cylindrical cell assembled with LiMn₂O₄ (LMO) cathode and Li₄Ti₅O₁₂ (LTO) anode with a high capacity of 1.3 Ah based on our developed FGPE (detailed in Figure S17a and Table S3). The rate performance in the voltage of 1.5-3.8 V is shown in Figure S17a. Impressively, a high discharge capacity of 1.3 Ah can be retained at 1 C, with an excellent cycle lifespan of 500 cycles and a high capacity retention of 71.0% (Figure 5e). Notably, as far as we know, this is the first report for industry-level solid-state 18650 cylindrical batteries. The safety of the solid-state 18650 cylindrical cell was also investigated by using industrial abuse procedures (nail penetration). As shown in Figure 5f and Video S1, the cylindrical cell using FGPE remained intact during nail penetration without explosion or leakage, demonstrating its high safety. This also indicates that the outstanding performance originates from the improved compatibility between the solid electrolyte and electrodes, as a result of our developed fluorinated and crosslinked polyether electrolyte.

Conclusion

For the first time, a fluorinated and crosslinked polyether electrolyte, FGPE, has been designed and fabricated in this work, exhibiting excellent oxidation stability. By introducing the electron-withdrawing trifluoromethyl group, the HOMO of polyether becomes more negative, resulting in a significantly improved oxidation potential of 5.1 V. The fluorinated polymer network and the anion-rich solvation structure contributes to a SEI enriched with inorganic species and enhanced lithium metal stability. Additionally, a uniform and thin CEI is constructed, which leads to restrained electrolyte consumption and alleviated cathode cracking. In combination with the in-situ CROP method, FGPE simultaneously possesses a robust electrolyte network, high ionic conductivity (3.98 mS cm⁻¹), and compact interfacial contact with electrodes. As a result, the Li|FGPE|NCM622 battery exhibits one of the longest lifespan of 1000 cycles (78.0% capacity retention) among all the reported polymer electrolytes-based batteries.

Furthermore, FGPE represents the first reported polyether electrolyte that can be applied in 4.7 V NCM622 battery, achieving a high specific capacity of 210.2 mAh g⁻¹. Furthermore, our designed FGPE enabled solid-state lithium metal pouch cell with a high-loading (21 mg cm⁻¹), and industry-level 18650 cylindrical cell (1.3 Ah) with an outstanding cycling stability of 500 cycles. Our work provides an effective strategy of adopting polyether as oxidation-stable polymer electrolyte by fluorination and crosslinking, which may inspire the development of practical high-voltage solid-state LMBs.

Supporting Information

Supporting Information is available from the Wiley Online Library or from the author.

Acknowledgements

The authors gratefully acknowledge the financial support from National Natural Science Foundation of China (NSFC, 52090034), Ministry of Science and Technology of China (MoST, 2020YFA0711500), and the Higher Education Discipline Innovation Project (B12015).

Keywords: solid polymer electrolyte, in-situ crosslinking, fluorinated electrolyte, long cycling, high-voltage

Reference:

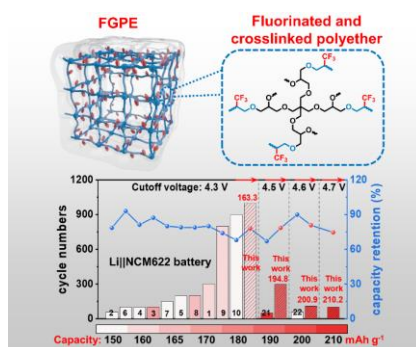
- [1] a) N. Kim, Y. Kim, J. Sung, J. Cho, *Nat. Energy* **2023**, *8*, 921; b) J. Liu, J. Zhang, J. Zhu, R. Zhao, Y. Zhang, Y. Ma, C. Li, H. Zhang, Y. Chen, *Nano Res.* **2023**, *16*, 12601; c) W. Zhao, K. Zhang, F. Wu, X. Wang, R. Guo, K. Zhang, Y. Yuan, Y. Bai, C. Wu, *Chem. Eng. J.* **2023**, *453*, 139348.
- [2] a) J. Ding, Y. Zhang, R. Xu, R. Zhang, Y. Xiao, S. Zhang, C. Bi, C. Tang, R. Xiang, H. S. Park, Q. Zhang, J. Huang, *Green Energy Environ.* **2023**, *8*, 1509; b) S. Nanda, A. Gupta, A. Manthiram, *Adv. Energy Mater.* **2020**, *11*, 2000804; c) S. Kim, G. Park, S. J. Lee, S. Seo, K. Ryu, C. H. Kim, J. W. Choi, *Adv. Mater.* **2023**, *35*, 2206625.
- [3] a) M. Yeddala, L. Rynearson, B. L. Lucht, *ACS Energy Lett.* **2023**, *8*, 4782; b) S. Qi, M. Li, Y. Gao, W. Zhang, S. Liu, J. Zhao, L. Du, *Adv. Mater.* **2023**, *35*, 2304951; c) C. Luo, H. Hu, T. Zhang, S. Wen, R. Wang, Y. An, S. S. Chi, J. Wang, C. Wang, J. Chang, Z. Zheng, Y. Deng, *Adv. Mater.* **2022**, *34*, 2205677.

- [4] a) J. Wang, S. Li, Q. Zhao, C. Song, Z. Xue, *Adv. Funct. Mater.* **2020**, *31*, 2008208; b) G. Xi, M. Xiao, S. Wang, D. Han, Y. Li, Y. Meng, *Adv. Funct. Mater.* **2020**, *31*, 2007598; c) M. Shen, Z. Wang, D. Cheng, H. Cheng, H. Xu, Y. Huang, *eTransportation* **2023**, *18*, 100264.
- [5] a) M. A. Cabañero Martínez, N. Boaretto, A. J. Naylor, F. Alcaide, G. D. Salián, F. Palombardini, E. Ayerbe, M. Borrás, M. Casas - Cabanas, *Adv. Energy Mater.* **2022**, *12*, 2201264; b) S. Xiao, L. Ren, W. Liu, L. Zhang, Q. Wang, *Energy Storage Mater.* **2023**, *63*, 102970; c) K. Hiraoka, M. Inoue, K. Takahashi, K. Hayamizu, M. Watanabe, S. Seki, *J. Electrochem. Soc.* **2021**, *168*, 060501.
- [6] a) X. Chen, X. Li, L. Luo, S. He, J. Chen, Y. Liu, H. Pan, Y. Song, R. Hu, *Adv. Energy Mater.* **2023**, *13*, 2301230; b) J. Li, Y. Ji, H. Song, S. Chen, S. Ding, B. Zhang, L. Yang, Y. Song, F. Pan, *Nanomicro Lett* **2022**, *14*, 191.
- [7] a) Y. Chen, Y. Cui, S. Wang, Y. Xiao, J. Niu, J. Huang, F. Wang, S. Chen, *Adv. Mater.* **2023**, *35*, 2300982; b) M. Jiang, D. L. Danilov, R. A. Eichel, P. H. L. Notten, *Adv. Energy Mater.* **2021**, *11*, 2103005; c) S. Park, G. Choi, H. Y. Lim, K. M. Jung, S. K. Kwak, N.-S. Choi, *ACS Appl. Mater. Interfaces* **2023**, *15*, 33693; d) Z. Shadiké, Y. Chen, E. Hu, J. Zhang, X.-Q. Yang, *Trends Chem.* **2023**, *5*, 775.
- [8] X. Yang, M. Jiang, X. Gao, D. Bao, Q. Sun, N. Holmes, H. Duan, S. Mukherjee, K. Adair, C. Zhao, J. Liang, W. Li, J. Li, Y. Liu, H. Huang, L. Zhang, S. Lu, Q. Lu, R. Li, C. V. Singh, X. Sun, *Energy Environ. Sci.* **2020**, *13*, 1318.
- [9] a) Z. Fang, Y. Luo, H. Liu, Z. Hong, H. Wu, F. Zhao, P. Liu, Q. Li, S. Fan, W. Duan, J. Wang, *Adv. Sci.* **2021**, *8*, e2100736; b) J. Zhu, J. Zhang, R. Zhao, Y. Zhao, J. Liu, N. Xu, X. Wan, C. Li, Y. Ma, H. Zhang, Y. Chen, *Energy Storage Mater.* **2023**, *57*, 92; c) H. T. Xu, H. R. Zhang, J. Ma, G. J. Xu, T. T. Dong, J. C. Chen, G. L. Cui, *ACS Energy Lett.* **2019**, *4*, 2871; d) K. Zhang, F. Wu, X. Wang, L. Zheng, X. Yang, H. Zhao, Y. Sun, W. Zhao, Y. Bai, C. Wu, *Adv. Funct. Mater.* **2021**, *32*, 2107764.
- [10] a) J. Xiang, Y. Zhang, B. Zhang, L. Yuan, X. Liu, Z. Cheng, Y. Yang, X. Zhang, Z. Li, Y. Shen, J. Jiang, Y. Huang, *Energy Environ. Sci.* **2021**, *14*, 3510; b) C. Z. Zhao, Q. Zhao, X. Liu, J. Zheng, S. Stalin, Q. Zhang, L. A. Archer, *Adv. Mater.* **2020**, *32*, e1905629.
- [11] H. Yang, B. Zhang, M. Jing, X. Shen, L. Wang, H. Xu, X. Yan, X. He, *Adv. Energy Mater.* **2022**, *12*, 2201762.
- [12] a) G. Zhou, J. Yu, F. Ciucci, *Energy Storage Mater.* **2022**, *55*, 642; b) Z. Weidong, S. Han, X. Xiaoxin, H. Qiu, W. Zhaoxu, C. Kejun, L. Xiaolei, G. Jian, L. Yutao, L. Hong, Q. Jieshan, *Angew.*

- Chem. Int. Ed.* **2021**, *60*, 18335; c) Y. Wang, S. Chen, Z. Li, C. Peng, Y. Li, W. Feng, *Energy Storage Mater.* **2022**, *45*, 474.
- [13] a) J. Guo, X. Liu, X. Cao, X. Zhang, H. Zhang, Y. Lu, C. Zhang, X. Zhang, *ACS Energy Lett.* **2023**, *8*, 4218; b) C. Zhang, Z. Lu, M. Song, Y. Zhang, C. Jing, L. Chen, X. Ji, W. Wei, *Adv. Energy Mater.* **2023**, *13*, 2203870; c) Y. Tian, S. Tan, C. Yang, Y. Zhao, D. Xu, Z. Lu, G. Li, J. Li, X. Zhang, C. Zhang, J. Tang, Y. Zhao, F. Wang, R. Wen, Q. Xu, Y. Guo, *Nat. Commun.* **2023**, *14*, 7247.
- [14] a) G. Xiao, H. Xu, C. Bai, M. Liu, Y. B. He, *Interdiscip. Mater.* **2023**, *2*, 609; b) Q. Liu, L. Wang, X. He, *Adv. Energy Mater.* **2023**, *13*, 2300798; c) Y. Han, Y. Zhou, J. Zhu, Z. Sun, L. Xu, C. Li, Y. Ma, H. Zhang, Y. Chen, *Sci. China Mater.* **2020**, *63*, 2344.
- [15] J. Xiao, Q. Li, Y. Bi, M. Cai, B. Dunn, T. Glossmann, J. Liu, T. Osaka, R. Sugiura, B. Wu, J. Yang, J.-G. Zhang, M. S. Whittingham, *Nat. Energy* **2020**, *5*, 561.
- [16] a) Q. Wang, C. Zhao, J. Wang, Z. Yao, S. Wang, S. G. H. Kumar, S. Ganapathy, S. Eustace, X. Bai, B. Li, M. Wagemaker, *Nat. Commun.* **2023**, *14*, 440; b) K. Zhang, F. Wu, X. Wang, S. Weng, X. Yang, H. Zhao, R. Guo, Y. Sun, W. Zhao, T. Song, X. Wang, Y. Bai, C. Wu, *Adv. Energy Mater.* **2022**, *12*, 2200368.
- [17] a) M. M. Jia, C. Zhang, Y. W. Guo, L. S. Peng, X. Y. Zhang, W. W. Qian, L. Zhang, S. J. Zhang, *Energy Environ. Mater.* **2022**, *5*, 1294; b) S.-D. Han, J. L. Allen, E. Jónsson, P. Johansson, D. W. McOwen, P. D. Boyle, W. A. Henderson, *J. Phys. Chem. C* **2013**, *117*, 5521.
- [18] Y. Huijun, Q. Yu, C. Zhi, H. ping, Z. Haoshen, *Angew. Chem. Int. Ed.* **2021**, *60*, 17726.
- [19] Q. Sun, Z. Cao, Z. Ma, J. Zhang, W. Wahyudi, T. Cai, H. Cheng, Q. Li, H. Kim, E. Xie, L. Cavallo, Y.-K. Sun, J. Ming, *ACS Mater. Lett.* **2022**, *4*, 2233.
- [20] X. Peng, B. Liu, J. Chen, Q. Jian, Y. Li, T. Zhao, *ACS Energy Lett.* **2023**, *8*, 3586.
- [21] Z. Xueying, H. Liqiang, L. Wei, W. Haotian, D. Yiming, L. Xuyang, W. Zhongqiang, Z. Honghe, H. Yunhui, *ACS Energy Lett.* **2021**, *6*, 2054.
- [22] a) J.-n. Duan, Q. Hou, R.-m. Yuan, J. Fan, M. Zheng, Q. Dong, *J. Mater. Chem. A* **2023**, *11*, 548; b) H. Gao, N. S. Grundish, Y. Zhao, A. Zhou, J. B. Goodenough, *Energy Mater. Adv.* **2021**, *2021*, 1932952.
- [23] Z. Li, S. Weng, J. Fu, X. Wang, X. Zhou, Q. Zhang, X. Wang, L. Wei, X. Guo, *Energy Storage Mater.* **2022**, *47*, 542.
- [24] P. Bai, X. Ji, J. Zhang, W. Zhang, S. Hou, H. Su, M. Li, T. Deng, L. Cao, S. Liu, X. He, Y. Xu, C. Wang, *Angew. Chem. Int. Ed.* **2022**, *61*, e202202731.

- [25] Y. Liu, M. Wang, J. Chen, J. Yang, K. Wang, Z. Ren, W. Xi, Y. Huang, J. Zheng, X. Li, *Sustain. Energy Fuels* **2020**, *4*, 2875.
- [26] a) B. Xu, L. Kong, G. Wen, M. G. Pecht, *IEEE Access* **2021**, *9*, 66687; b) W. Diao, S. Saxena, M. G. Pecht, *IEEE Access* **2020**, *8*, 21326; c) D. P. Finegan, E. Darcy, M. Keyser, B. Tjaden, T. M. M. Heenan, R. Jervis, J. J. Bailey, N. T. Vo, O. V. Magdysyuk, M. Drakopoulos, M. Di Michiel, A. Rack, G. Hinds, D. J. L. Brett, P. R. Shearing, *Adv. Sci.* **2017**, *5*, 1700369.

Entry for the Table of Contents



A fluorinated and crosslinked polyether electrolyte (FGPE) exhibiting excellent oxidation stability was developed, which enabled the polymer electrolyte-based Li||LiNi_{0.6}Co_{0.2}Mn_{0.2}O₂ batteries to achieve the longest cycling of 1000 cycles and high operating voltage of 4.7 V. Notably, solid-state industry-level 18650 cylindrical cells were first reported with an outstanding stability (500 cycles).